Organic Electronics 40 (2017) 36–41

Contents lists available at ScienceDirect

Organic Electronics

journal homepage: www.elsevier.com/locate/orgel

High efficiency polymer solar cells based on alkylthio substituted benzothiadiazole-quaterthiophene alternating conjugated polymers

Zhe Zhang [a], Zhen Lu [b], Jicheng Zhang [a], Yahui Liu [a], Shiyu Feng [a], Liangliang Wu [a], Ran Hou [a], Xinjun Xu [a,*], Zhishan Bo [a,**]

[a] Beijing Key Laboratory of Energy Conversion and Storage Materials, College of Chemistry, Key Laboratory of Theoretical and Computational Photochemistry, Ministry of Education, Beijing Normal University, Beijing 100875, China
[b] College of Chemistry and Chemical Engineering, Shanxi Datong University, Datong 037009, China

ARTICLE INFO

Article history:
Received 20 September 2016
Received in revised form
19 October 2016
Accepted 21 October 2016

Keywords:
Conjugated polymer
Organic solar cells
Donor and acceptor
Low bandgap polymer
Photovoltaic

ABSTRACT

We have designed and synthesized two alkylthio substituted benzothiadiazole-quaterthiophene based conjugated polymers (**P1** and **P2**) and investigated their photovoltaic performances. Theoretical simulation has demonstrated that the introduction of alkylthio substituents can increase the planarity of the resulted conjugated polymers. The fluorinated polymer **P1** possesses a deeper HOMO energy level than the non-fluorinated polymer **P2** and can form well-developed fibril networks when blended with $PC_{71}BM$. PSCs based on **P1**:$PC_{71}BM$ (1:1.2, by weight) gave a PCE of 7.76% with a V_{oc} of 0.69 V, a J_{sc} of 16.30 mA cm^{-2} and an FF of 0.69. Our results have demonstrated that alkylthiothiophene could be a useful building block for the construction of high efficiency polymer donor materials used for PSCs.
© 2016 Elsevier B.V. All rights reserved.

1. Introduction

Polymer solar cells (PSCs) have received more and more attention in recent years because of their good solution processability and mechanical flexibility, which potentially allow them to be fabricated by more convenient and low-cost processes such as roll-to-roll printing or inkjet printing [1–8]. To accomplish the goal of application, the development of novel active layer materials has played an important role in improving the device performance. Within which, the progress of low band-gap (LBG) D-A conjugated polymer donors has helped to significantly enhance the power conversion efficiency (PCE) of PSCs because of their tunable band gaps and energy levels [9–21]. Among the reported LBG polymers, benzothiadiazole-quaterthiophene based polymers usually afford high PCEs [22–36].

Generally, a variety of molecular design strategies have been used in tuning the band gap and energy level of polymer donors. For example, altering the side chains of conjugated polymers can tune their energy levels, their solubility in the processing solvent, and their morphology in the active layer [37–39]. Recently, thienyl-substituted or phenyl-substituted benzodithiophenes carrying alkylthio chains have been used as building blocks for the synthesis of polymer donors [20,21,25,36,40,41]. Compared with alkyl/alkoxy chains, alkylthio chains have been demonstrated to be more effective in tuning the HOMO levels of most conjugated polymers. For instance, Li's group have reported a series of 5-alkylthiothienyl substituted benzodithiophene based polymers. Compared with 5-alkylthienyl or 5-alkoxythiothienyl substituted benzodithiophene based analogues, the V_{oc} of devices was enhanced from 0.78 or 0.74 V–0.84 V [25]. Hou's group have reported a series of conjugated polymers, which yielded an enhancement of V_{oc} in ~0.15 V in comparison with the 4,5-bis(alkylthio)thienyl substituted benzodithiophene based analogues [36]. Our group have reported synthesized a series of 4-(alkylthio)phenyl substituted benzodithiophene based conjugated polymers, which gave an impressive PCE of 7.7% when blended with $PC_{71}BM$ as the active layer and a PCE of 10.4% in ternary PSCs with ITIC and $PC_{71}BM$ as the acceptors [20,21]. However, up to now, the reported alkylthio substituents are all confined to benzodithiophene groups. Although benzodithiophene unit is a very attractive building block to construct high-performance polymer donors, it suffers from rapid degradation due to the photooxidation in air at the 4- and 8-

* Corresponding author.
** Corresponding author.
E-mail address: xuxj@bnu.edu.cn (X. Xu).

http://dx.doi.org/10.1016/j.orgel.2016.10.032
1566-1199/© 2016 Elsevier B.V. All rights reserved.

positions [42]. To the best of our knowledge, the photovoltaic performance of 4-alkylthio substituted benzothiadiazole-quaterthiophene based conjugated polymers has never been exploited yet. Herein, we have synthesized two benzothiadiazole-quaterthiophene based conjugated polymers (**P1** and **P2**) comprising 4-alkylthio substituents as side chains, and demonstrated by theoretical simulation that the introduction of alkylthio substituent can significantly increase the planarity of polymer backbones in comparison with their alkyl/alkoxy substituted counterparts. The fluorinated polymer **P1** possesses a deeper HOMO energy level and can form well-developed fibril network morphology when blended with $PC_{71}BM$. And **P1** based PSCs gave a PCE of 7.76% with a V_{oc} of 0.69 V, a J_{sc} of 16.30 mA cm^{-2} and an FF of 0.69.

2. Results and discussion

2.1. Material synthesis and characterization

The syntheses of **M1**, **M2**, **P1** and **P2** are outlined in Scheme 1 and the concrete procedures are provided in the Supporting Information. Compound **1** was synthesized according to the reported procedure [43]. Compounds **4**, **5** and **8** were purchased from Suna.Tech. Inc.. Starting from commercially available 3-bromothiophene, its treatment with *n*-butyllithium (*n*-BuLi) was followed by quenching the formed 3-thienyl anion with sublimed sulfur to afford thiophene-3-thiol (**1**) in a yield of 88%. The reaction of compound **1** and 1-bromo-2-octyldodecane with potassium *tert*-butoxide as the base in anhydrous ethanol gave compound **2** in a yield of 96%. The subtraction of the proton at the 2-position of thiophene ring in compound **2** with lithium dimethylamide (LDA) was followed by reaction with tri(*n*-butyl)tin chloride to give compound **3**, which was directly used for the next step without further purification. Stille cross-coupling of compound **3** and 4,7-dibromo-5,6-difluoro-2,1,3-benzothiadiazole (**4**) using $Pd_2(dba)_3$ and $P(o\text{-tol})_3$ as the catalyst precursors and THF as the solvent furnished compound **6** in a yield of 77%. Bromination of compound **6** with *N*-bromosuccinimide (NBS) in CH_3Cl_3 gave **M1** in almost quantitative yield. Polymer **P1** was synthesized in a yield of 70% by Stille cross-coupling reaction of **M1** and compound **8** using $Pd(PPh_3)_4$ as the catalyst precursor in a solvent mixture of toluene and *N*,*N*-dimethylformamide (DMF) at 110 °C. Similarly, compound **7**, **M2** and polymer **P2** were synthesized. **P1** is insoluble in commonly used organic solvents such as chlorobenzene (CB), *o*-dichlorobenzene (DCB) at room temperature, but can be fully soluble at elevated temperature; whereas **P2** is fully soluble in the above mentioned organic solvents at room temperature. Molecular weights and their distributions of **P1** and **P2** were obtained by gel permeation chromatography (GPC) using CB as an eluent at 130 °C with narrowly distributed polystyrenes as calibration standards, and the results are summarized in Table S1. Thermal properties of **P1** and **P2** were investigated by thermogravimetric analysis (TGA) under a nitrogen atmosphere. As shown in Fig. S2, **P1** and **P2** displayed a very good thermal stability with the 5% decomposition temperature up to 345 and 310 °C, respectively. The differential scanning calorimetry (DSC) test was performed from 80 °C to 250 °C at the heating rate of 10 °C/min under a nitrogen atmosphere. The DSC traces in Fig. S3 showed no obvious glass transition for these two polymers. The packing of polymer chains as film was characterized using small angle X-ray diffraction (SAXRD) method. As shown in Fig. 1, **P1** exhibited three diffraction peaks in the XRD curves. The first peak, which reflected the distance of polymer backbones separated by the flexible side chains, is located at 2θ of 7.91°, corresponding to a distance of 11.17 Å. The peak located at 2θ of 24.75° in the wide angle region reflects the π-π stacking distance of 3.59 Å between polymer backbones [26]. In contrast to the polymer with the same length of alkyl side chain reported in the literature which has a lamellar stacking distance of 19.0 Å and a π-π stacking distance of 3.70 Å, our alkylthio substituted polymer shows a more closely packing [19]. This result may be attributed to the F···S interaction which could improve inter/intramolecular interaction of polymer chains [44]. As for **P2**, two diffraction peaks were observed in the XRD curve. The first peak located at 2θ of 7.53° in the small angle region reflected the distance of polymer backbones separated by the flexible side chains, which is corresponding to a distance of 11.72 Å. The second peak, which reflected the π-π stacking distance between polymer backbones, are located at 2θ of

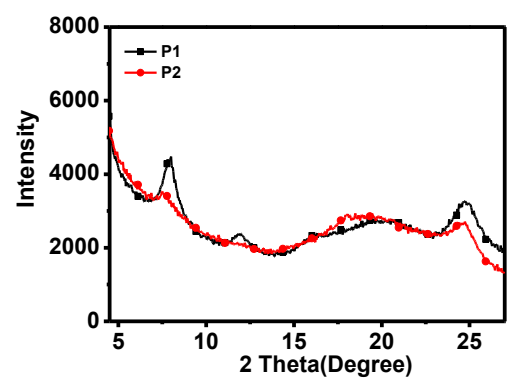

Fig. 1. Film XRD curves of **P1** and **P2**.

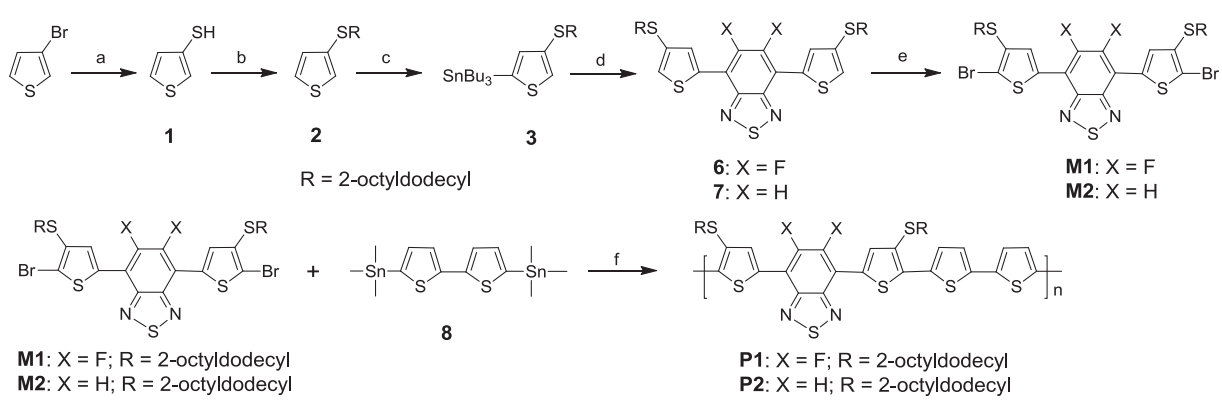

Scheme 1. Synthetic route to polymers **P1 and P2.** (a) BuLi, S_8, Et_2O; (b) $(CH_3)_3COK$, RBr, EtOH; (c) LDA, Tri(*n*-butyl)tin chloride, THF; (d) 4,7-dibromo-5,6-difluorobenzothiadiazoel (4) or 4,7-dibromobenzothiadiazole (5), $Pd_2(dba)_3$, $P(o\text{-tol})_3$,THF; (e) NBS, CH_3Cl_3; (f) $Pd(PPh_3)_4$, toluene/DMF.

24.57°, corresponding to a distance of 3.62 Å. In the wide angle region, the diffraction peak of **P1** become more acute than **P2**, which could reflect that crystallinity of polymers is improved when F atom is incorporated into the polymer backbone. The appropriate increase of crystallinity contributes to the improvement of the specific nanoscale morphology of the active layer. This is also consistent with the results of morphology characterizations [45,46]. Density functional theory (DFT) calculations at the B3LYP/6-31G(d) level were also used to investigate the molecular simulation of **P1** and **P2** are shown in Fig. 2. For simplicity, methyl substituents were used for the calculation instead of 2-octyldodecyl chains. Compared with the alkyl substituted polymer in Fig. 2 (c), alkylthio substituted polymers (**P1** and **P2**) showed better planar conformation, which would lead to extended π-conjugation and enhanced intermolecular interactions.

2.2. Optical properties and electrochemical properties

Optical properties of **P1** and **P2** were investigated by UV–vis absorption spectroscopy. As shown in Fig. 3a, **P1** and **P2** in DCB solutions at 100 °C displayed similar absorption spectra with two absorption peaks located at 450 and 629 nm for **P1** and 433 and 600 nm for **P2**. In going from solution to film, the two absorption peaks are red-shifted to 451 and 649 nm with a new should peak at 691 nm as shown in Fig. 3b, indicating that **P1** form stronger interchain interactions in the solid state. For **P2** as film, the two absorption peaks were red-shifted to 449 and 629 nm as shown in Fig. 3b. No should peak was observed in the long wavelength region indicated that **P2** film is more amorphous. The onsets of film absorption for **P1** and **P2** were determined to be 780 and 775 nm, respectively. The band gaps of **P1** and **P2** were therefore calculated to be 1.59 and 1.60 eV, respectively, according to the equation: $E_{g,opt} = 1240/\lambda_{onset}$. Electrochemical properties of **P1** and **P2** were investigated by cyclic voltammetry (CV) using a standard three-electrode electrochemical cell and the CV curves are shown in Fig. 4. The highest occupied molecular orbital (HOMO) energy levels of **P1** and **P2** were determined using the equation $E_{HOMO} = -e(E_{ox} + 4.71)$ to be −5.28 and −5.25 eV, respectively, indicating that the fluorine atom substitution can lower the HOMO energy level of polymers. Consequently, devices fabricated with **P1** are expected to show higher V_{oc} than those fabricated with **P2**. The lowest unoccupied molecular orbital (LUMO) energy levels of **P1** and **P2** were calculated according to the equation $E_{LUMO} = E_{HOMO} + E_{g,opt}$ to be −3.69 and −3.65 eV, respectively. The optical data, energy levels and band gaps are also summarized in Table 1.

2.3. Photovoltaic properties

To evaluate the photovoltaic performance of **P1** and **P2**, PSCs were fabricated with the conventional device configuration of indium tin oxide (ITO)/poly(3,4-ethylenedioxythiophene): poly(styrenesulfonate) (PEDOT:PSS)/polymer:$PC_{71}BM$/LiF/Al. The weight ratio of polymer to $PC_{71}BM$, the morphology of the active

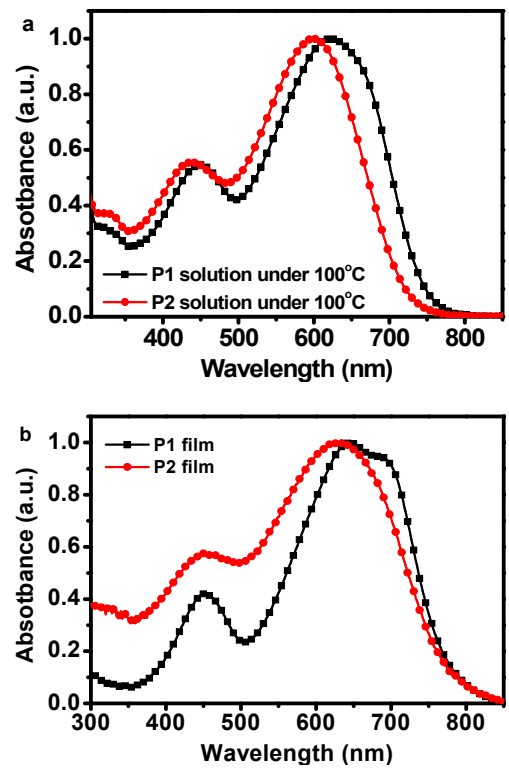

Fig. 3. UV–visible absorption spectra of **P1** and **P2** in DCB solutions at 100 °C (a) and as films (b).

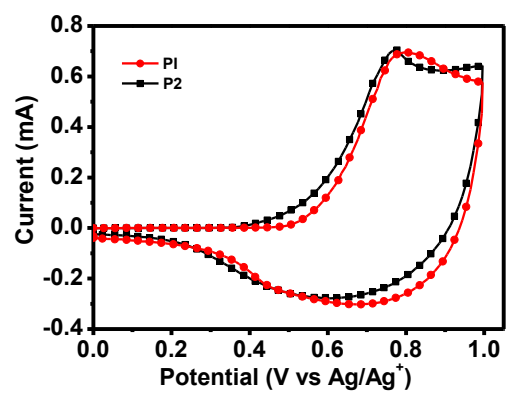

Fig. 4. Cyclic voltammograms of copolymers **P1** and **P2** in films on a platinum electrode in 0.1 mol/L Bu_4NPF_6 acetonitrile solution at a scan rate of 100 mV/s.

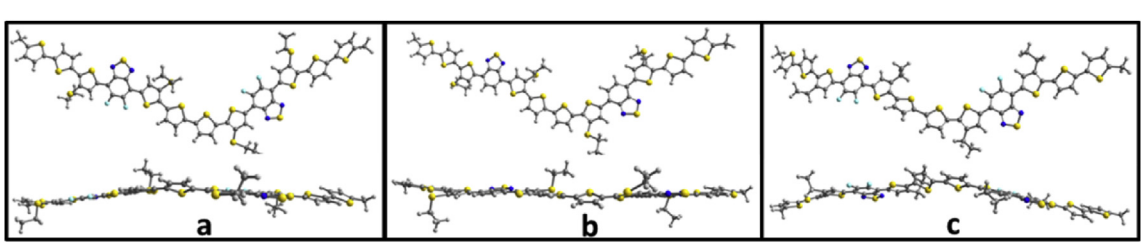

Fig. 2. Molecular geometry of the polymers with methyl groups replacing the alkyl substituents to simplify the calculations: a, **P1**; b, **P2**; c, alkylthio side chains of **P1** was replaced by the same alky side chains (yellow, sulfur; green, fluorine; blue, nitrogen). (For interpretation of the references to colour in this figure legend, the reader is referred to the web version of this article.)

Table 1
Physical, electronic, and optical properties of **P1** and **P2.**

Polymer	T_d[a] (°C)	λ (nm) solution	λ (nm) film	$E_{g,opt}$[b] (eV)	HOMO (eV)	LUMO (eV)
P1	345	450, 629	451, 649, 691	1.59	−5.28	−3.69
P2	310	433, 600	449, 629	1.60	−5.25	−3.65

[a] T_d is the 5% weight-loss temperature under N_2 atmosphere.
[b] Calculated from the onset absorption of **P1** and **P2**, $E_{g,opt} = 1240/\lambda_{onset}$.

layer and thickness of the active layer were optimized. Since additive can influence the morphology of active layer, the content of 1,8-diiodooctane (DIO) was also screened. The optimal devices were fabricated from a solution of polymer and $PC_{71}BM$ in CB and DCB (1:1, v/v) containing 2.5% of DIO as the additive, and the polymer concentration is 9 mg ml^{-1} and the D/A ratio is 1:1.2. In order to completely dissolve the polymer, the blend solution was stirred at 110 °C for at least 5 h. Both the blend solutions and the ITO substrates were preheated to 110 °C in a glove box before spin-coating the active layer. And the active layers were annealed at 80 °C for 10 min before being transferred to the vacuum chamber of thermal evaporator inside the same glove box.

The current density-voltage (*J-V*) curves of the best performance devices fabricated with and without DIO (2.5%) under AM 1.5G illumination are shown in Fig. 5a. For **P1**, devices fabricated from CB + DCB solutions with and without 2.5% DIO gave PCEs of 7.76% and 5.22%, respectively; whereas for **P2**, devices fabricated from CB + DCB solutions with and without 2.5% DIO gave PCEs of 2.02% and 1.75%, respectively. The device parameters are also summarized in Table 2. As expected, the fluorinated polymer **P1** exhibited larger J_{sc} and higher FF than non-fluorinated polymer **P2**. The fluorinated polymers usually exhibited higher charge carrier mobility than the corresponding non-fluorinated polymers because of their enhanced

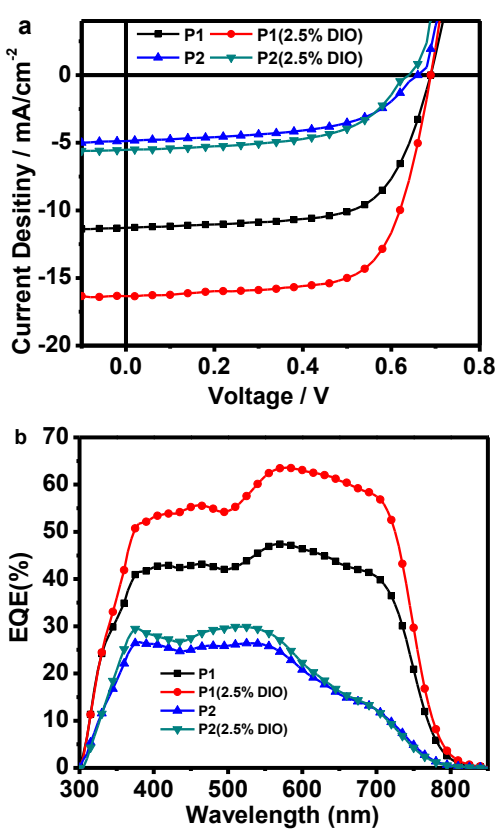

Fig. 5. *J-V* curves (a) and EQE spectra (b) of polymer/$PC_{71}BM$ solar cells.

inter/intra molecular interactions, which usually lead to well-developed fibril structure (vide infra) in the active layer [19,42]. In addition, **P1** based devices also exhibited slightly higher V_{oc} than **P2** based devices because of its slightly deeper HOMO energy level. Consequently, **P1** exhibited higher PCE than **P2**. Compared with the donor polymer with the same backbone but substituted by alkyl groups (polymer FH) reported in the literature, under the condition of a similar device structure alkylthio substituted polymer (**P1**) showed a better PCE than FH (6.4% reported in the reference) [19]. Although Yan's group has reported that alkyl substituted polymer (FH) shows a higher PCE than this work, it should be noted that the device structure is different with this work [10].

External quantum efficiencies (EQEs) of optimized devices measured under monochromatic light are shown in Fig. 5 b. When using 2.5% DIO as the processing additive, **P1** exhibited higher EQEs (above 50%) than **P2** in the range of 400–730 nm, indicating a more efficient photo conversion process and a more balanced charge transportation in devices. The Jsc values obtained from the integration of EQE curves are consistent with the J_{sc} obtained from *J-V* measurements. Hole mobilities of blend films fabricated under the optimized conditions were characterized by space charge limited current (SCLC) method, the curve shown in Fig. S4. The **P1**:$PC_{71}BM$ and **P2**:$PC_{71}BM$ blend films exhibited hole mobilities of 4.73×10^{-4} and 4.40×10^{-5} cm^2 v^{-1} s^{-1}, respectively. The polymer **P1** shows a higher hole mobility than **P2**, which can be attributed to the F atom, because F atom can suppress bimolecular recombination as well as improve specific nanoscale morphology of active blends [44,46]. The SCLC mobility results are quite consistent with the measured J_{sc} and PCEs.

2.4. Film morphologies

The morphology of blend films fabricated under optimized conditions was investigated by atomic force microscopy (AFM) in tapping mode and transmission electron microscope (TEM) and the AFM and TEM images are shown in Figs. 6 and 7, respectively. As shown in Fig. 6, the morphologies of **P1**:$PC_{71}BM$ and **P2**:$PC_{71}BM$ blend films were of some difference. **P1** in the blend film formed fibrils and showed a good miscibility with $PC_{71}BM$; whereas **P2** in the blend film formed larger aggregates and exhibited apparent phase separation with $PC_{71}BM$. For the **P1**:$PC_{71}BM$ blend film, the formation of more homogeneous morphology with well-developed interconnected network structure can be more easily observed in the TEM images as shown in Fig. 7. For the **P2**:$PC_{71}BM$ blend film, it can be clearly seen that larger aggregates were formed from the TEM images as shown in Fig. 7. The morphology difference was probably caused by the solubility difference of these two polymers in the processing solvent. For **P1**, the poor solubility made it precipitated firstly to form nanofibrils during the drying of the blend films. The formation of nanofibrils can further prevent the formation of large aggregates by $PC_{71}BM$ during the drying of the blend films; whereas for **P2**, $PC_{71}BM$ molecules might precipitate firstly to form larger spherical aggregates as shown in Fig. 7 due to the good solubility of **P2** in the processing solvent. As reported in the literature, the formation of phase separation in nanoscale for the donor and acceptor in the blend film is beneficial for charge

Table 2
Photovoltaic performances of Polymer:$PC_{71}BM$ blend films.

Polymer	Solvent	V_{oc} (V)	J_{sc} (mA cm^{-2})	*FF*	PCE (%) best/ave[b]	Thickness (nm)
P1	CB + DCB	0.69	11.30	0.67	5.22/5.01	/
	CB + DCB[a]	0.69	16.30	0.69	7.76/7.61	136
P2	CB + DCB	0.64	4.88	0.56	1.75/1.67	/
	CB + DCB[a]	0.63	5.52	0.58	2.02/1.98	105

[a] With 2.5% DIO, by volume.
[b] The average PCEs were based on ten devices.

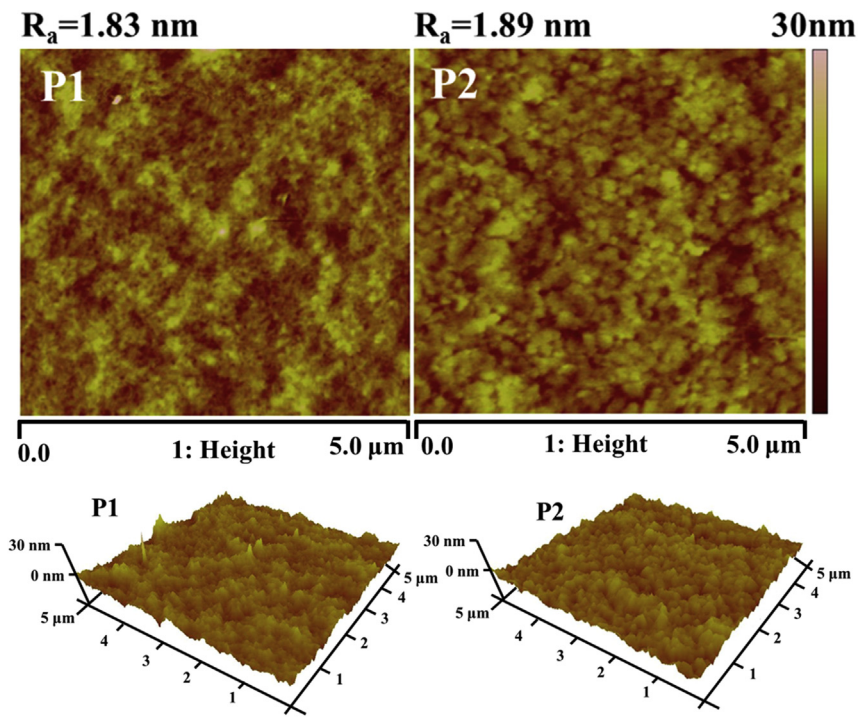

Fig. 6. AFM images of **P1**:$PC_{71}BM$ and **P2**:$PC_{71}BM$ blend films fabricated under optimized conditions.

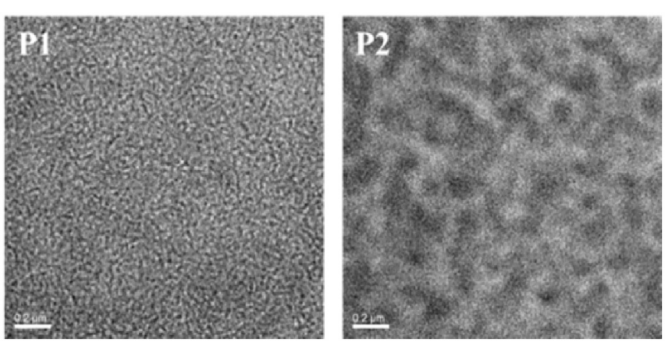

Fig. 7. TEM images of **P1**:$PC_{71}BM$ and **P2**:$PC_{71}BM$ blend films fabricated under optimized conditions, the scale bar is 0.2 μm.

carrier generation and transportation. The marked morphology difference of the active layer showed a significant influence on the performance of photovoltaic devices. The device results can be well illustrated by the investigation of morphology of blend films.

3. Conclusions

In summary, we have designed and synthesized two novel conjugated polymers (**P1** and **P2**) comprising two alkylthio substituted thiophene units in each repeating unit. As demonstrated by molecular simulation, the alkylthio substituted polymers (**P1** and **P2**) showed a more planar conformation than those alkyl substituted polymers. PSCs with the blend of **P1**:$PC_{71}BM$ (1:1.2, by weight) as the active layer showed a PCE of 7.76% with a V_{oc} of 0.69 V, a J_{sc} of 16.30 mA cm^{-2} and an FF of 0.69 under AM 1.5G illumination. In comparison with the non-fluorinated counterpart **P2**, the fluorinated polymer **P1** possesses a deeper HOMO energy level and can form well-developed fibril network morphology when blended with $PC_{71}BM$. And fluorinated polymer **P1** based PSCs showed higher PCEs than non-fluorinated polymer **P2**. Our results have demonstrated that 3-alkylthiothiophene could be a useful building block for the construction of high efficiency polymer donor materials used for PSCs.

Acknowledgements

Financial support from the NSF of China (91233205 and 21574013), Program for Changjiang Scholars and Innovative Research Team in University and the Fundamental Research Funds for the Central Universities are gratefully acknowledged.

Appendix A. Supplementary data

Supplementary data related to this article can be found at http://

dx.doi.org/10.1016/j.orgel.2016.10.032.

References

[1] G. Yu, J. Gao, J. Hummelen, F. Wudl, A. Heeger, Science 270 (1995) 1789.
[2] R. Søndergaard, M. Hösel, D. Angmo, T. Larsen-Olsen, F. Krebs, Mater. today 15 (2012) 36.
[3] X. Guo, N. Zhou, S. Lou, J. Smith, D. Tice, J. Hennek, R. Ortiz, J. Navarrete, S. Li, J. Strzalka, Nat. Photonics 7 (2013) 825.
[4] G. Li, V. Shrotriya, J. Huang, Y. Yao, T. Moriarty, K. Emery, Y. Yang, Nat. Mater. 4 (2005) 864.
[5] C. Gao, Z. Qiao, K. Shi, S. Chen, Y. Li, G. Yu, X. Li, H. Wang, Org. Electron. 38 (2016) 245.
[6] J. You, L. Dou, K. Yoshimura, T. Kato, K. Ohya, T. Moriarty, K. Emery, C. Chen, J. Gao, G. Li, Nat. Commun. 4 (2013) 1446.
[7] A. bin Mohd Yusoff, D. Kim, H. Kim, F. Shneider, W. da Silva, J. Jang, Energy Environ. Sci. 8 (2015) 303.
[8] T. Hu, P. Jiang, L. Chen, K. Yuan, H. Yang, Y. Chen, Org. Electron. 37 (2016) 35.
[9] Z. He, C. Zhong, S. Su, M. Xu, H. Wu, Y. Cao, Nat. Photonics 6 (2012) 591.
[10] Y. Liu, J. Zhao, Z. Li, C. Mu, W. Ma, H. Hu, K. Jiang, H. Lin, H. Ade, H. Yan, Nat. Commun. 5 (2014) 5293.
[11] Z. Wu, C. Sun, S. Dong, X. Jiang, S. Wu, H. Wu, H. Yip, F. Huang, Y. Cao, J. Am. Chem. Soc. 138 (2016) 2004.
[12] H. Hu, K. Jiang, G. Yang, J. Liu, Z. Li, H. Lin, Y. Liu, J. Zhao, J. Zhang, F. Huang, J. Am. Chem. Soc. 137 (2015) 14149.
[13] V. Tamilavan, S. Kim, R. Agneeswari, D. Lee, S. Cho, Y. Jin, J. Jeong, S. Park, M. Hyun, Org. Electron. 38 (2016) 283.
[14] C. Duan, F. Huang, Y. Cao, J. Mater. Chem. 22 (2012) 10416.
[15] G. Li, R. Zhu, Y. Yang, Nat. Photonics 6 (2012) 153.
[16] Z. Chen, P. Cai, J. Chen, X. Liu, L. Zhang, L. Lan, J. Peng, Y. Ma, Y. Cao, Adv. Mater. 26 (2014) 2586.
[17] D. Dang, X. Wang, Y. Zhi, L. Meng, X. Bao, R. Yang, W. Zhu, Org. Electron. 32 (2016) 237.
[18] J. Jheng, Y. Lai, J. Wu, Y. Chao, C. Wang, C. Hsu, Adv. Mater. 25 (2013) 2445.
[19] J.W. Jo, S. Bae, F. Liu, T. Russell, W. Jo, Adv. Funct. Mater. 25 (2015) 120.
[20] X. Gong, G. Li, C. Li, J. Zhang, Z. Bo, J. Mater. Chem. A 3 (2015) 20195.
[21] H. Lu, J. Zhang, J. Chen, Q. Liu, X. Gong, S. Feng, X. Xu, W. Ma, Z. Bo, Adv. Mater. (2016), http://dx.doi.org/10.1002/adma.201603588.
[22] H. Wang, Y. Zhu, Z. Liu, L. Zhang, J. Chen, Y. Cao, Org. Electron. 31 (2016) 1.
[23] M. Zhang, X. Guo, S. Zhang, J. Hou, Adv. Mater. 26 (2014) 1118.
[24] S. Zhang, L. Ye, J. Hou, Adv. Energy Mater. (2016) 1502529.
[25] C. Cui, W. Wong, Y. Li, Energy Environ. Sci. 7 (2014) 2276.
[26] G. Li, X. Gong, J. Zhang, Y. Liu, S. Feng, C. Li, Z. Bo, ACS Appl. Mater. Inter. 8 (2015) 3686.
[27] D. Khatiwada, S. Venkatesan, Q. Chen, J. Chen, N. Adhikari, A. Dubey, A. Mitul, L. Mohammed, Q. Qiao, J. Mater. Chem. A 3 (2015) 15307.
[28] C. Cui, Z. He, Y. Wu, X. Cheng, H. Wu, Y. Li, Y. Cao, W. Wong, Energy Environ. Sci. 9 (2016) 885.
[29] H. Yao, H. Zhang, L. Ye, W. Zhao, S. Zhang, J. Hou, Macromolecules 48 (2015) 3493.
[30] S. Zhang, B. Yang, D. Liu, H. Zhang, W. Zhao, Q. Wang, C. He, J. Hou, Macromolecules 49 (2015) 120.
[31] H. Yao, W. Zhao, Z. Zheng, Y. Cui, J. Zhang, Z. Wei, J. Hou, J. Mater. Chem. A 4 (2016) 1708.
[32] B. Xu, Z. Zheng, K. Zhao, J. Hou, Adv. Mater. 28 (2016) 434.
[33] Z. Zheng, S. Zhang, M. Zhang, K. Zhao, L. Ye, Y. Chen, B. Yang, J. Hou, Adv. Mater. 27 (2015) 1189.
[34] Y. Liu, W. Zhao, Y. Wu, J. Zhang, G. Li, W. Li, W. Ma, J. Hou, Z. Bo, J. Mater. Chem. A 4 (2016) 8097.
[35] Z. Zhang, X. Zhang, J. Zhang, X. Gong, Y. Liu, H. Lu, C. Li, Z. Bo, RSC Adv. 6 (2016) 39074.
[36] H. Yao, H. Zhang, L. Ye, W. Zhao, S. Zhang, J. Hou, ACS Appl. Mater. Inter. 8 (2015) 3575.
[37] H. Yao, L. Ye, B. Fan, L. Huo, J. Hou, Sci. China Mater. 58 (2015) 213.
[38] J. Mei, Z. Bao, Chem. Mater. 26 (2013) 604.
[39] Z.G. Zhang, Y. Li, Sci. China Chem. 58 (2015) 19.
[40] X.P. Xu, K. Feng, K. Li, Q. Peng, J. Mater. Chem. A 3 (2015) 23149.
[41] K. Feng, X.P. Xu, Z.J. Li, Y. Li, K. Li, T. Yu, Q. Peng, Chem. Commun. 51 (2015) 6290.
[42] S. Alem, S. Wakim, J. Lu, G. Robertson, J. Ding, Y. Tao, ACS Appl. Mater. Inter. 4 (2012) 2993.
[43] H. Bronstein, J. Frost, A. Hadipour, Y. Kim, C. Nielsen, R. Ashraf, B. Rand, S. Watkins, I. McCulloch, Chem. Mater. 25 (2013) 277.
[44] H.X. Zhou, L.Y. Yang, A.C. Stuart, S.C. Price, S.B. Liu, Wei You, Angew. Chem. Int. Ed. 50 (2011) 2995.
[45] K. Kim, S. Park, H. Yu, H. Kang, I. Song, J.H. Oh, B.J. Kim, Chem. Mater. 26 (2014) 6963.
[46] K. Li, Z.J. Li, K. Feng, X.P. Xu, L.Y. Wang, Q. Peng, J. Am. Chem. Soc. 135 (2013) 13549.